HUNTINGTON MEDICAL RESEARCH INSTITUTES
NEUROLOGICAL RESEARCH LABORATORY
734 Fairmount Avenue
Pasadena, California 91105

Contract No. N01-NS-8-2399
Quarterly Progress Report
Jan 1, 2000-March 31, 2000
Report No. 6

"Microstimulation of the Lumbosacral Spinal Cord"

Douglas B. McCreery, Ph. D.
Albert S. Lossinsky, Ph.D.
Ted G. F. Yuen, Ph.D..
Leo Bullara, B.A.
William F. Agnew, Ph.D.

SUMMARY AND ABSTRACT

We have continued to develop procedures for implanting our form-fitting microelectrode array into the feline sacral spinal cord. In this array, 6 discrete activated iridium microelectrodes extend from a circular array superstructure 3 mm in diameter. The underside of the superstructure is contoured into a saddle-shaped concavity, which straddles the convex dorsal surface of the sacral spinal cord. The arrays are implanted using a high speed inserter instrument which injects the arrays into the cord a velocity of 1 to 2 m/sec.

Stimulation regimens were initiated 30 or 31 days after implanting the microelectrodes. The stimulus waveform was cathodic-first, controlled-current, charge-balanced (biphasic) pulse pairs, in which the stimulus pulse amplitude reached 100 μA, and the pulse duration was a great as 400 μs (40 nC/phase). However, the pulsing rate was quite low (20Hz) and in some cases, the stimulus was administered only 20% of the time throughout the two 12-hours sessions.

After 12 to 24 hours of such stimulation, the histologic evaluation revealed a form of acute stimulation-induced tissue injury that we have observed only once previously in any of our microstimulation studies in the cerebral cortex, cochlear nucleus or spinal cord. The lesions were localized to within 200 μm of the microelectrode tip, and were characterized by a dense aggregation of glial cells and leukocytes. There was essentially total destruction and/or displacement of the neuropil and neurons that originally surrounded the electrode tip. The glial elements probably are astrocytes and the lymphocyte contingent apparently is composed of activated lymphocytes, with a few neutrophils and fewer monocytes. The number of lymphocytes is variable across animals, and the lesion is probably best characterized as a reactive astrocytosis.

In two of the animals in the present series (SP110 and SP111), we fabricated the lead wires from platinum/20% iridium, which has much greater tensile strength than the pure platinum used previously, but which is stiffer and much less malleable. To compensate, the distal 2 cm of the lead wires were coiled into a closely-wound helix, 1.1 mm in diameter. However the arrays equipped with these cables tended to become tipped and sometimes twisted after implantation. Clearly, these cables are too stiff and bulky for this application and a substitute material must be found. We will evaluate cables containing only 10% iridium, which will be more flexible and malleable.

In the present series we modified the protocol by which the electrodes are implanted with the custom inserter instrument. This was done to reduce the incidence of a particular type of gliotic scarring that appears to have been due to the electrodes momentarily overshooting their target during the insertion stroke. The modifications greatly reduced this type of injury.

METHODS

In the past quarter, we implanted 4 of the bilateral microelectrode arrays into the sacral spinal cords of 4 cats (SP109, SP110 and SP111 and SP112). In this report, we present the findings from SP109, SP110 and SP111.The iridium microelectrodes have active geometric surface areas of approximately 2,000 μm^2 at their tips. Six discrete activated iridium microelectrodes extend from a circular array superstructure 3 mm in diameter. The underside of the superstructure is contoured into a saddle-shaped concavity, which straddles the convex dorsal surface of the sacral spinal cord. This is intended to place their tips within the intermediolateral cell column of the S_2 sacral spinal cord when the array's concave bottom is centered over the cord's midline.

In previous animals, the lead wires had been composed of pure platinum, 50 μm in diameter, insulated with Teflon. On numerous occasions, these leads had broken during the 30 days after implantation of the arrays (the spinal cord is the only anatomical site in which we have encountered this problem). In the present series, we fabricated the leads from an alloy with much greater tensile strength (platinum/20% iridium) but this material is stiffer and much less malleable than is the pure platinum. To compensate, the distal 2 cm of the lead wires were coiled into a closely-wound helix, 1.1 mm in diameter. As noted in this report, this configuration has proved to be too bulky for this application and a substitute material must be found.

The arrays were implanted into the spinal cord at the S_2 or S_1 levels, using aseptic surgical techniques, with the cats anesthetized with halothane and nitrous oxide. The surgical procedure is described in detail in QPR #5. A recording electrode was inserted through a separate small opening in the dura and passed approximately 4 cm caudally, to lie adjacent to the ventral roots.

The microelectrode array was then placed into the end of the stator tube (barrel) of the inserter tool, where it is held against the armature by a vacuum. The array cable was secured loosely to the dura, approximately 2 cm rostral to the implant site. The orifice of the barrel was centered over the midline of the sacral cord, with the array cable extending rostrally or caudally.

On the basis of the histologic findings from previous animals, we made two modifications to the electrode insertion protocol. Firstly, the dorsal surface of the spinal cord was not "pre-dimpled" by the orifice of the inserter prior to inserting the array; the barrel was lowered until it just made contact with the cord. Secondly, the inserter instrument was adjusted so that the underside of the array button ("superstructure") was not expelled from the barrel at the end of the insertion stroke. There modifications were made in order to reduce a particular type of gliotic scarring that appears to have been due to the electrodes momentarily overshooting their target during the insertion stroke. In compensation for these changes, the insertion velocity was increased to approximately 2 m/sec, in

order to ensure complete insertion of the arrays.

Chronic stimulation protocols

Thirty-two to 33 days after the implant surgery, the 2-day stimulation regimens were initiated. The cats were anesthetized with Propofol and 4 or 5 of the 6 intraspinal microelectrodes were pulsed for 12 hours on each of two consecutive days. The stimulus waveform was cathodic-first, controlled-current, charge-balanced (biphasic) pulse pairs.

TABLE 1

Cat/ Days post-implant	Electrode	µA	Hz	Pulse width (µs/ph)	Charge/ph (nC)	Duty cycle (% on)
SP109 / 32-33	1	80	20	150	12	100/100
SP109 / 32-33	2	80	20	150	12	100/100
SP109 / 32-33	3	100	20	150	15	100/100
SP109 / 32-33	4	100	20	150	15	100/100
SP109 / 32-33	5	not pulsed				0/0
SP109 / 32-33	6	not pulsed				0/0
SP110 / 31-32	1	100	20	400	40	20/20
SP110 / 31-32	2	100	20	400	40	0/100
SP110 / 31-32	3	not pulsed				
SP110 / 31-32	4	100	20	400	40	20/20
SP110 / 31-32	5	100	20	400	40	100/100
SP110 / 31-32	6	100	20	400	40	100/0
SP111 / 30-31	1	100	20	400	40	100/100
SP111 / 30-31	2	not pulsed				0/0
SP111 / 30-31	3	100	20	400	40	20/20
SP111 / 30-31	4	not pulsed				0/0
SP111 / 30-31	5	100	20	400	40	100/100
SP111 / 30-31	6	100	20	400	40	20/20

(*)" Duty cycle" indicates the % of the time during the 2 day, 12-hr/day regimen that the particular electrode was pulsed. 100% indicates continuous pulsing. 20% indicate 10 seconds of pulsing, then 40 seconds without pulsing. The first and second values listed are the duty cycles used on day 1 and day 2, respectively. Thus 0/100 indicate no pulsing on day 1, 100 % duty cycle on day 2.

Animals SP110 and SP111 received stimuli whose charge per phase was much greater than had been used in previous animals. Our intent was to evaluate microstimulation protocols that are appropriate for inducing contraction of the urinary bladder. With a high charge per phase, the neurons within a fairly large volume of tissue can be excited with only one or two microelectrodes. With the high current density and high charge per phase, there is a risk of injury to the tissue very close to the electrode. However, we hypothesized that this risk would be reduced by the use of a reduced duty cycle (In a clinical prosthesis, the induction of urogenital functions in a patient with spinal cord injury would not require continuous stimulation).

Immediately after the end of the second day of stimulation, the animals were deeply anesthetized with pentobarbital and perfused through the aorta for 3 minutes with a prewash solution consisting of 300-900 ml of phosphate-buffered saline, and 0.05% procaine HCL, to remove blood. This was followed by either 4 L of ½ strength Karnovsky's Fixative in 0.1 M sodium phosphate buffer or 10 % neutral buffered formalin at pH 7.3. The sacral spinal cord was resected and the capsule of connective tissue covering the array matrix was removed, leaving the array *in situ.* The spinal roots and nerves were identified to determine the exact level of the array.

Tissue blocks were washed overnight in PBS and then for 2 hrs in distilled water to remove aldehyde fixatives not bound to the tissue proteins. After washing, the tissues were dehydrated in a graded series of ethanol, and embedded in paraffin. The paraffin-embedded tissue was cut at a thickness of 6-7μm and stained with Nissl and H & E stains.

RESULTS

Measurement of hydrostatic pressure within the urinary bladder

In cat SP110, we monitored the effect of microstimulation in the S_2 spinal cord on the hydrostatic pressure within the urinary bladder. Thirty days after implanting the electrode array, the cat was anesthetized with Propofol and the urinary bladder was catheterized. Hydrostatic pressure was measured with a micro-transducer (Miller Instruments, Model SPR524), and the data were digitized and stored in a PC computer. The bladder was evacuated, then filled with sterile saline, to a base pressure of approximately 10 mm Hg. The effect of electrical stimulation was recorded, for pulse rates ranging from 10 to 50 Hz, and for stimulus amplitudes of 5 to 40 nC/phase. The electrical stimulation was applied with a 25% duty cycle (15 seconds of stimulation, then 15 seconds without stimulation). Unilateral stimulation produced only a very small elevation of bladder pressure. However, bilateral stimulation (with electrode 1 and 4, pulsed in the interleaved mode) consistently produced an elevation of bladder pressure. These electrodes were close to the intermediolateral cell column in S_2 A high stimulus amplitude (40 nC/phase, 2,000 $\mu C/cm^2$) was required to produce the

maximum pressure elevation. Figure 1 shows a plot of the hydrostatic pressure within the urinary bladder. The height of the upper trace is proportional to stimulus charge per phase X pulse rate. When the stimulus amplitude was 100 μA and the pulse duration was 400 μs/phase (40 nC/phase), a pulsed rate of 10 Hz produced an initial elevation of bladder pressure, a transient decrease, then a secondary increase. Stimulating at 20 Hz produced a larger increase in pressure, but stimulation at a higher rate did not produce a greater increase. In spite of the rather high stimulus amplitude, we did not observe any co-contraction of somatic musculature, either in the limbs or in the trunk or abdomen. Based on these findings, we evaluated, in cats SP110 and SP111, the histologic effects of prolonged stimulation using 40 μC/phase and a pulse rate of 20 Hz.

Histologic Findings

In two cats (SP109, SP111) subcutaneous infections were associated with the long cables traversing from the percutaneous connector to the lumbosacral region. Histological analysis of the surrounding tissue indicated a chronic inflammation consisting of a mixture of neutrophils, mononuclear cells and phagocytes.

Fourteen of 16 electrode tips were located in the histologic sections from the three cats. The tips were located within the vicinity of the intermediolateral cell column (ICC). Some of the electrode tips were within the column, while most electrodes were slightly medial to the ICC. Only one electrode (SP110, electrode #4) showed evidence of having transiently penetrated past its final depth. This improvement from our previous series probably is due to our modification of the protocol for inserting the electrodes.

The tissue surrounding the tips of unpulsed electrodes appeared to be generally healthy, with some minimal acellular gliotic scarring. There were unequivocal stimulation-induced changes in the neuropil surrounding the tips of the pulsed electrodes. The severity of the injury increased with the amplitude of the stimulus (12-15 nC/phase, vs 40 nC/ph), but at the highest amplitude, the correlation between severity and duty cycle (100%, vs 20%) was somewhat equivocal. The tip sites were surrounded by dense aggregates of glial cells (presumable astrocytes), with variable numbers of leukocytes (mostly lymphocytes). Neuronal changes associated with high-amplitude stimulation ranged from neuronal hyperchromicity or slight darkening to total neuronal loss (no histological evidence of neurons within 200 μm of the tips). These changes were not observed adjacent to unpulsed tips. Other histological changes included increased neovascularization. In one electrode that penetrated into the ventral funiculus, there was more extensive gliotic scarring and increased vasculitis associated with meningeal vessels. In animals SP110 and SP111, the dorsal cord surface was compressed on one side, indicating that the array had become tipped after implantation.

Specific Changes:

SP109. Figure 2 shows the electrode array in situ, after fixation. Figure 3 also shows the array from SP111 described in detail below. The two rows of electrodes were nearly parallel to the midline of the spinal cord, and the array matrix (superstructure) is not conspicuously tipped to either side. The histological evaluation of the tissue surrounding the unpulsed electrodes revealed thin gliotic capsules surrounding the electrode tracks, a few astrocytes, some minimal acellular gliotic scarring, neovascularization and normal-appearing neurons (Figures 4, 5). The tips of electrodes pulsed at 80 to 100 μA, 150 μs/phase (12 to 15 nC/phase) were surrounded by a few lymphocytes intercalated into the capsule and within the neuropil surrounding the tips, as well as reactive astrocytes (Figures 6, 7). The histologic features varied from one electrode to another. In some cases, there was a paucity of neurons immediately surrounding the electrode tips. In other cases, the neurons were hyperchromatic (Figure 7). Neurons greater than 200 μm distant from the E tips appeared normal.

SP 110. In this animal, there were profound tissue changes associated with the high-amplitude stimulation (100 μA, 400 μs/phase, 20% or 100% duty cycle). The histologic changes surrounding unpulsed electrode #3 were similar to those around the unpulsed electrodes in SP109. One difference was that several leukocytes, including small round lymphocytes and neutrophils were close to the tip. Adjacent venules also presented small perivascular cuffs that also included neutrophils (Figures 8, 9). The remaining 5 pulsed electrodes were surrounded by dense aggregates of leukocyte, and there were numerous leukocytes surrounding post capillary venules and small veins, both near and distant to the electrode tips (Figures 10, 11, 13). The leukocyte cell types, in the order of decreasing frequency, were small lymphocytes, neutrophils and mononuclear cells. Some larger veins distant from the pulsed electrodes were cuffed primarily by lymphocytes (Figure 12). Neuronal changes immediately adjacent to the pulsed electrode tips ranged from varying degrees of hyperchromicity to edematous or vacuolated cells with perineuronal edematous changes (Figures 14-16). The latter were observed up to 500 μm from the tip sites (Figure 16). Within the cellular aggregates immediately surrounding the tips sites, no neurons or even remnants of neurons could be discerned.

SP111. Four of the electrode in this animal were pulsed at high amplitude (100 μA, 400 μs/phase) and with duty cycles of 20% or 100%. There were few leukocytes and little reactive gliosis around the tip of unpulsed electrode #4 tip and only a small, acellular gliotic scar was present (Figures 17, 18). Neurons near the tip appeared normal or slightly swollen. The exact sites of the tips of electrodes #1 #2 were not evaluated in this animal due to technical problems during preparation of the material, but adjacent sections were available. Leukocytic infiltrates were observed in the neuropil adjacent to pulsed electrode #1 but not adjacent to unpulsed electrode #2. The leukocytic

infiltrates and reactive gliosis were greatest around the tips of electrodes #1 and #5, which were pulsed with the highest duty cycle (Figures 19-21). The tips of electrodes pulsed with the 20% duty cycle also were surrounded by leukocytic infiltrates and reactive gliosis (Figures 22-24). As in previous animals, a few of the neurons distant from pulsed and unpulsed electrodes were undergoing chromatolysis (Figure 25), probably as a result of transection of their axons by the electrode during implantation.

Immunohistochemistry. In SP111, some of the sections were stained for the immunohistochemical reaction to glial fibrillary acidic protein (GFAP), an astrocyte marker. GFAP was variably upregulated within astrocytes around the perimeter of the lesions surrounding pulsed electrode #1, #5 and #6, but not within the lesions themselves, which appear to be composed of reactive astrocytes and a few lymphocytes and neutrophils (Figure 26).

DISCUSSION

These studies were conducted in order to examine the issues that are attendant to microstimulation of the small parasympathetic neurons of the intermediolateral cell column of the S_2 spinal cord, which innervate the detrusor muscle of the urinary bladder. We found that in order to achieve a significant rise in bladder pressure via microstimulation with only a single (bilateral) pair of electrodes, a high stimulus pulse amplitude and pulse duration are desirable. After 12 to 24 hours of such stimulation, we observed a form of acute stimulation-induced tissue injury that we have observed only once previously in any of our microstimulation studies in the cerebral cortex, cochlear nucleus or spinal cord. The injury was induced by prolonged, low-rate (20 Hz), high amplitude stimulation, with a duty cycle as low as 20% (10 seconds with stimulation, 40 seconds without stimulation repeated continuously). The lesion is localized to within 200 μm of the microelectrode tip, and is characterized by a dense aggregation of glial cells and leukocytes. There is essentially total disruption and/or displacement of the neuropil and neurons that originally surrounded the electrode tips. The glial elements probably are astrocytes and the lymphocyte contingent apparently is composed of activated lymphocytes, with a few monocytes. The number of lymphocytes is variable between animals, and the lesion is probably best characterized as a reactive astrocytosis. However, the cellular aggregates do not contain detectable amounts of glial fibrillary acidic protein (GFAP), although this protein is increased within the neuropil surrounding the lesion. A decrease in GFAP may occur early in CNS lesions, and this probably reflects injured or dying astrocytes (Chen et al, 1993; Norenberg, 1994). Neurons and remnants of neurons cannot be discerned within the lesion, while immediately surrounding the cellular aggregates, the neurons are somewhat shrunken and stellate, and others are undergoing chromatolysis.

This tissue injury was induced by stimulation regimens in which some of the parameters are considerably greater than those that we have employed in any of our previous studies. The long pulse duration (400 μs/ph, cathodic-first pulse pairs) and the high pulse current (100 μA) yield a charge per phase of 40 nC, an average charge density of approximately 2,000 μC/cm² and an average current density of approximately 5 A/cm² at the electrode-tissue interface (based on an electrode surface area of approximately 2,000 +/- 400 μm²). However, at the tips of the electrodes, where the radius of curvature is smallest, the current density and charge density will be higher than these average values. It remains to be determined which of the stimulus parameters is linked most closely to the injury. In the course of our studies of prolonged microstimulation in the feline cochlear nucleus, we have noted a similar (albeit milder) type of reactive gliosis surrounding the tips of microelectrodes that were pulsed with short-duration, high amplitude pulse pairs, suggesting that current density is an important factor in the induction of this type of injury. In the CN, the problem appears to have been eliminated by doubling the electrode surface area, to 2,000 μm^2. However, in the CN, the current density reach 6.3 A/cm^2, (greater than in these spinal cord studies), but the reactive gliosis was much milder. Also, the same current density was used in SP109, SP110 and SP111, but the injury was much greater in the latter two animals, in which the charge per phase and charge density was greater, due to the longer pulse duration. This implicates charge density and/or charge per phase.

In the cochlear nucleus, prolonged high-rate (500 Hz) microstimulation at a much lower charge per phase (4 nC) induces vacuolations of the myelinated axons in the neuropil surrounding the microelectrode tips. We have not observed this type of injury in the spinal cord. It may occur with only with high-rate stimulation or perhaps it is associated with the particular neural anatomy of the ventral cochlear nucleus.

In a clinical prosthesis, electromicturition or other urogenital functions would require only a few minutes of stimulation per day. During the next quarter, we will investigate stimulus regimens in which the duty cycle is less than the 20% used in the experiments reported here. We also will investigate the use of electrodes with larger surface areas, which will reduce the current and charge density at the electrode-tissue interface. However, it is possible that a spatially extensive population of neurons can be activated safely by microstimulation only by distributing the stimulus over a number of microelectrodes.

In the three cats described in this report, the procedure for implanting the electrodes was modified slightly. Firstly, the dorsal surface of the spinal cord was not "pre-dimpled" by the orifice of the inserter instrument, prior to inserting the array. Instead, the barrel was lowered until it just made contact with the cord. Secondly, the inserter instrument was adjusted so that the underside of the

array button ("superstructure") was not expelled from the barrel at the end of the insertion stroke. In cat SP109, the revised protocol for inserting the electrodes substantially reduced the amount of gliotic scarring around the electrodes tips, and the arrays were well-positioned atop the dorsal columns. In the other animals (SP110 and SP111), there also was minimal evidence of the type of "overshoot" injury which prompted us to change the protocol. However, another problem arose. In these cats, we fabricated the lead wires from platinum/20% iridium, which has much greater tensile strength than the pure platinum used previously, but which is stiffer and much less malleable. In compensation, the distal 2 cm of the lead wires were coiled into a close-wound helix, 1.1 mm in diameter. However, after implantation, these arrays tended to become tipped to one side and sometimes twisted about a dorso-ventral axis. Clearly, these cables are too stiff and bulky for this application and a substitute material must be found. We will evaluate cables containing only 10% iridium, which we be more flexible and malleable.

REFERENCES

Chen, H., Chopp, M.,Schultz, L., Bodzin, G., Garcia, J.H. (1993) Sequential neuronal and astrocyte changes after transient middle cerebral artery occlusion in the rat. J. Neurol. Sci. 118:109-116

Norenberg, M. (1994) Astrocyte responses to CNS injury (1994) J. Neuropath. & Exptl. Neurol. 53: 213-220

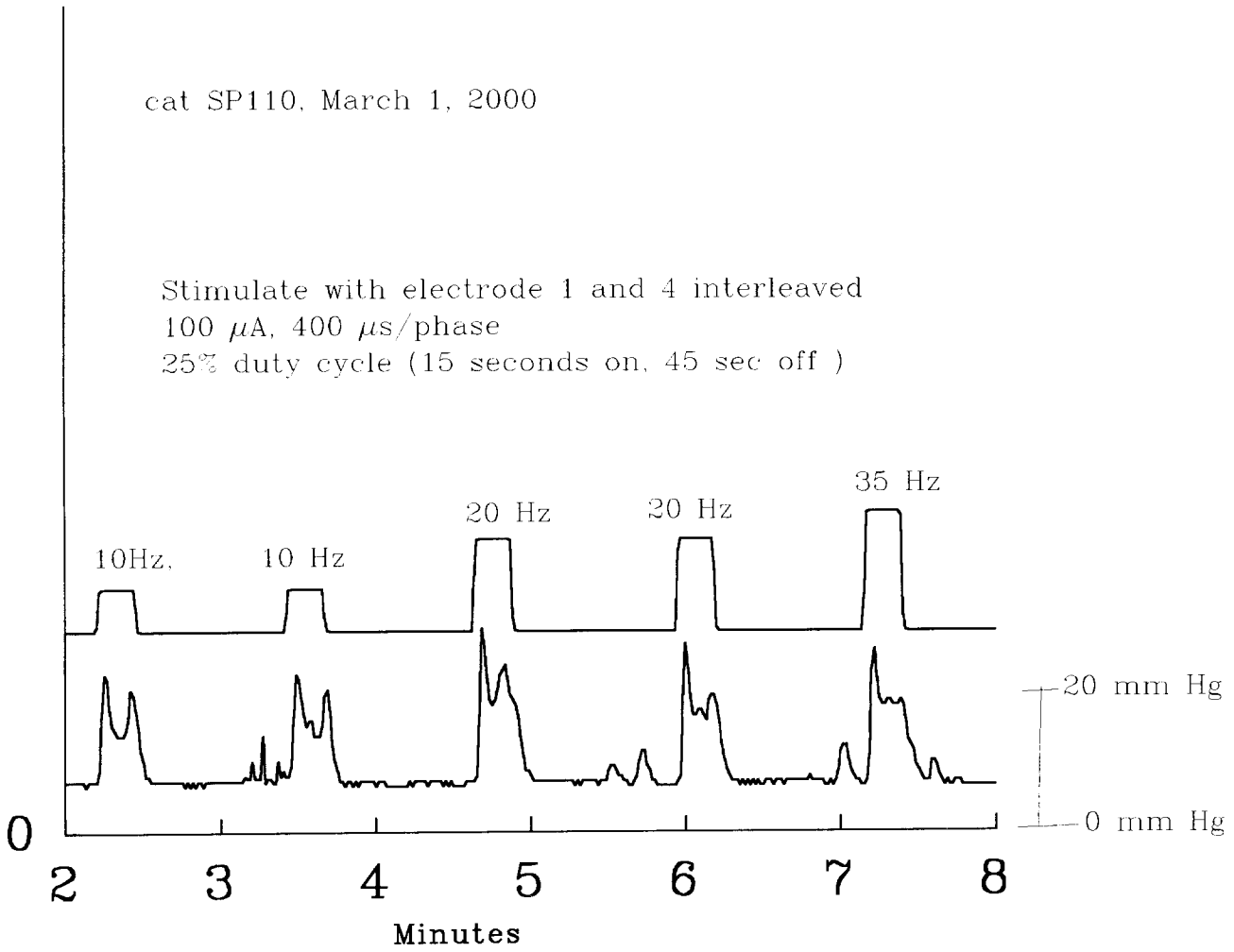

Figure 1

c:\data\spdata\sp110bm.spg

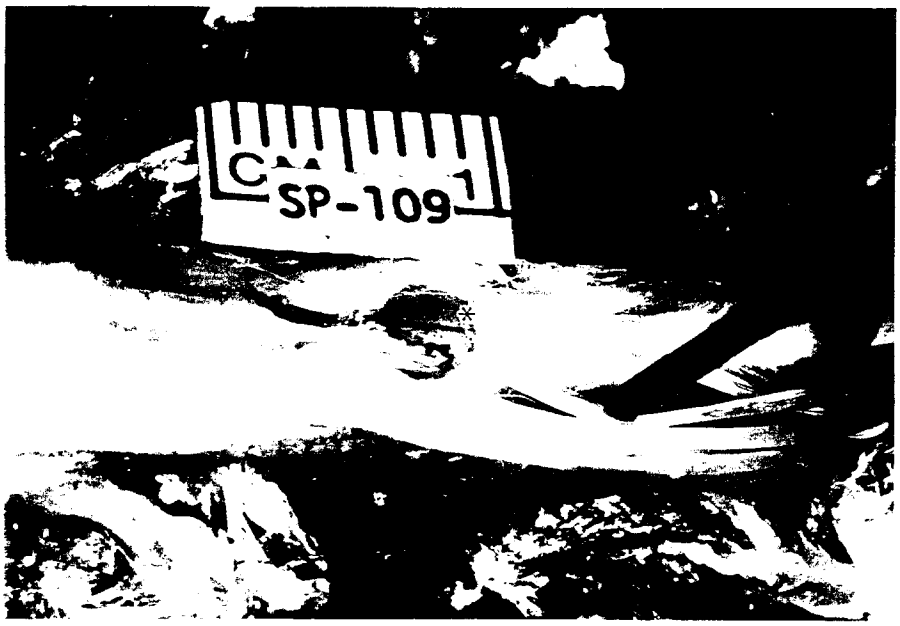

Figure 2. SP109. The 6-electrode array (*) at autopsy within the S_1-S_2 spinal cord, after vascular perfusion. Figures 4-25 stained with Nissl stain; Figure 26 stained with hematoxylin. Small rule divisions = 1 mm.

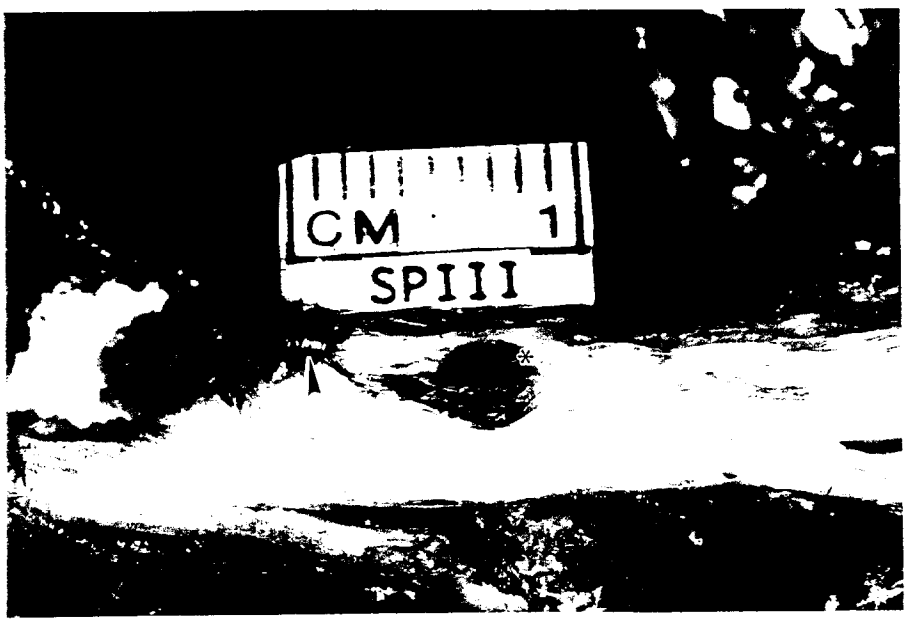

Figure 3. SP111. In this photograph also taken at autopsy, the array superstructure (*) is attached to the platinum-iridium lead wires, which are formed into a tight coil (arrowhead).

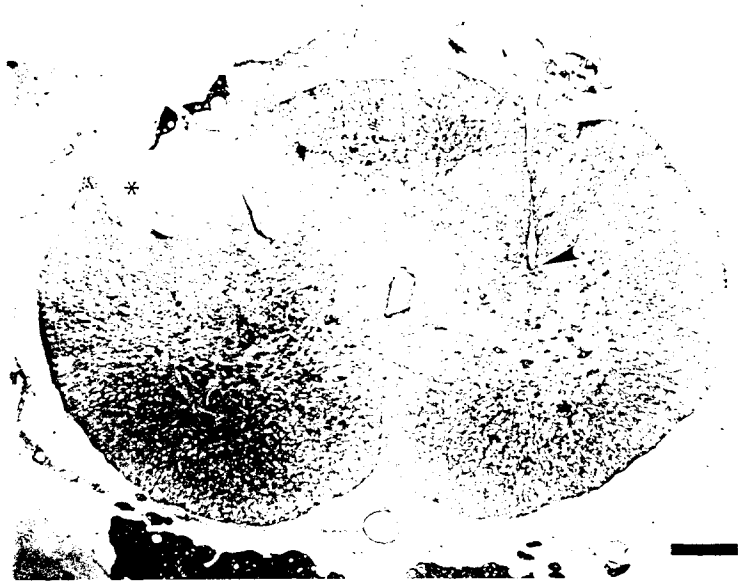

Figure 4. SP109. The track of unpulsed electrode # 6. Note the site of the electrode tip (arrowhead) and the compression of the dorsal surface of the cord, on the side opposite to the electrode track (*). Bar = 500 µm.

Figure 5. SP109. Higher magnification of the site of the tip of unpulsed electrode #6 (T). The tissue within 200 µm of the tip appears normal (arrowheads). Note the neovascularization (v) and reactive astrocytes along the track of the electrode shaft (arrow). Bar = 50 µm.

Figure 6. SP109. The track of pulsed electrode #4. Note the electrode tip (arrowhead) and the minimal compression of the cord's dorsal surface(*). Stimulus parameters: 20 Hz, 100 µA, 150 us/phase, 100% duty cycle. Bar = 500 µm.

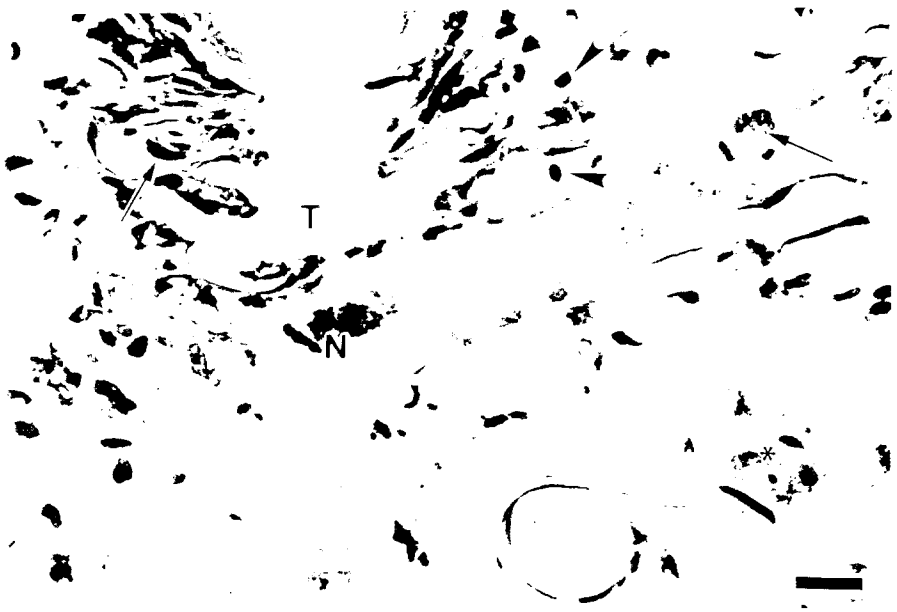

Figure 7. SP109. High magnification of the tip (T) of pulse electrode #4. Note the dark cell (presumably a damaged neuron, N), several reactive astrocytes (arrows), and small round lymphocytes (arrowheads). A normal-appearing neuron (*) is 200 µm from the tip. Bar = 50 µm.

Figure 8. SP110. The site of the tip of the unpulsed electrode # 3 (arrowhead). There was minimal compression of the dorsal surface of the sacral cord. Bar = 500 µm.

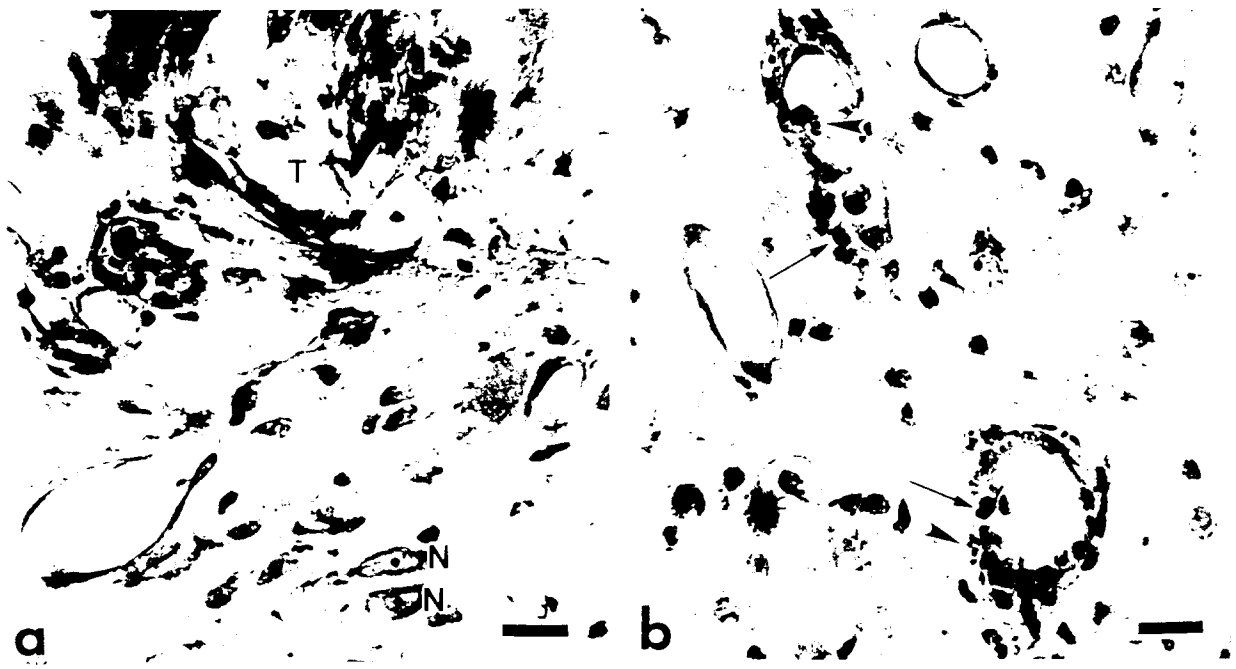

Figure 9. SP110. a. Higher magnification of the tissue in the vicinity of the tip (T) of unpulsed electrode #3. Note the normal appearing neurons (N) within 200 µm of the tip. b. Perivascular cuffing of neutrophils (arrowheads) and lymphocytes (arrows) surrounding veins. Bars = 50 µm.

Figure 10. SP110. The site of the tips of pulsed electrodes #1 and #6 (arrowheads). Also note the perivascular infiltrates of inflammatory cells associated with several large and small blood vessels (*). Bar = 500 µm.

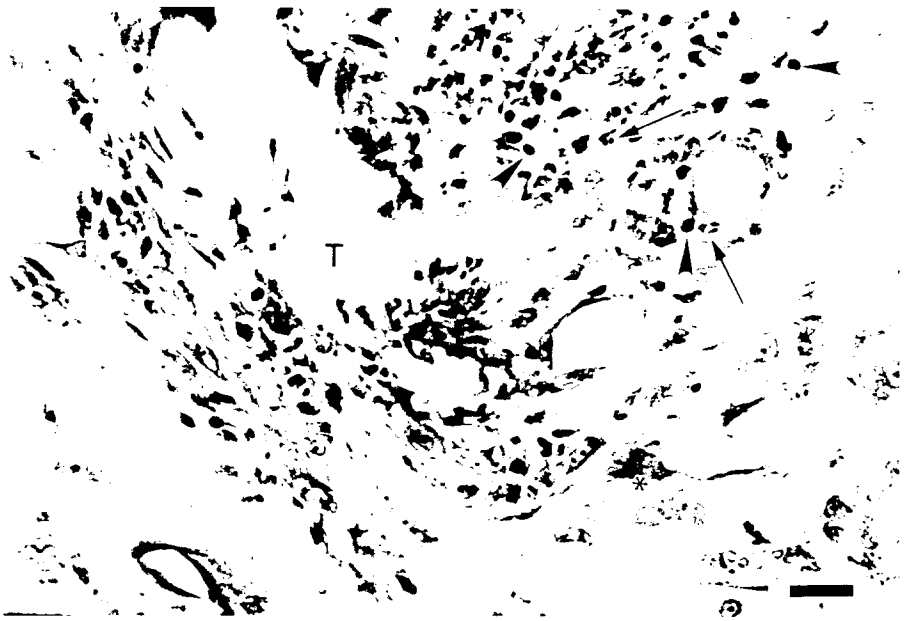

Figure 11. SP110. High magnification view showing the site of the tip (T) of pulsed electrode #6. The site is surrounded by scattered lymphocytes (arrowheads) and perivascular cuffs composed of neutrophils (arrows) and lymphocytes. Neuronal changes include darkening of the soma (*). Stimulus parameters: 20 Hz, 100 µA, 400 µs/phase. 100% duty cycle, (1st day only). Bar = 50 µm.

Figure 12. SP110. High magnification of the perivascular cuff shown in Figure 10. Note the heavy accumulation of inflammatory cells (mostly lymphocytes, *) surrounding the blood vessel. Bar = 50 µm.

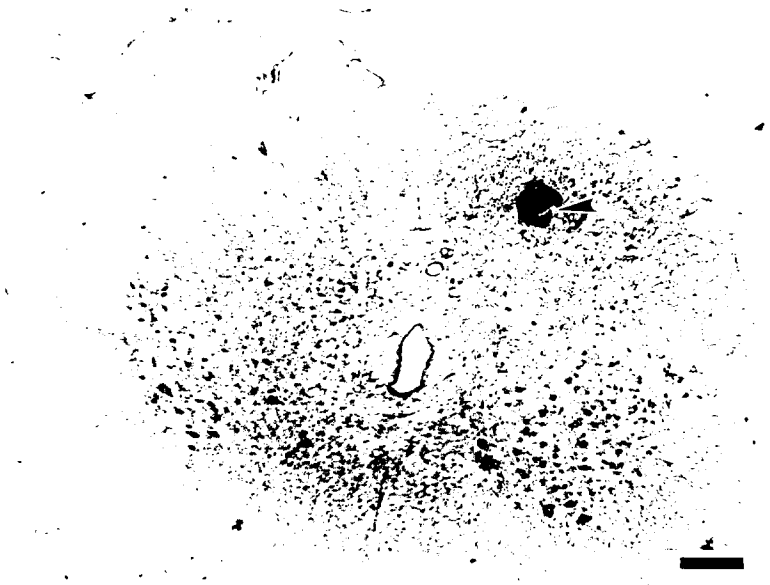

Figure 13. SP110. The site of the tip of pulsed electrode #2 is surrounded by leukocytes (arrowhead). Stimulus parameters: 20 Hz, 100 µA, 400 µs/phase, 100% duty cycle. (2nd day only) Bar = 500 µm.

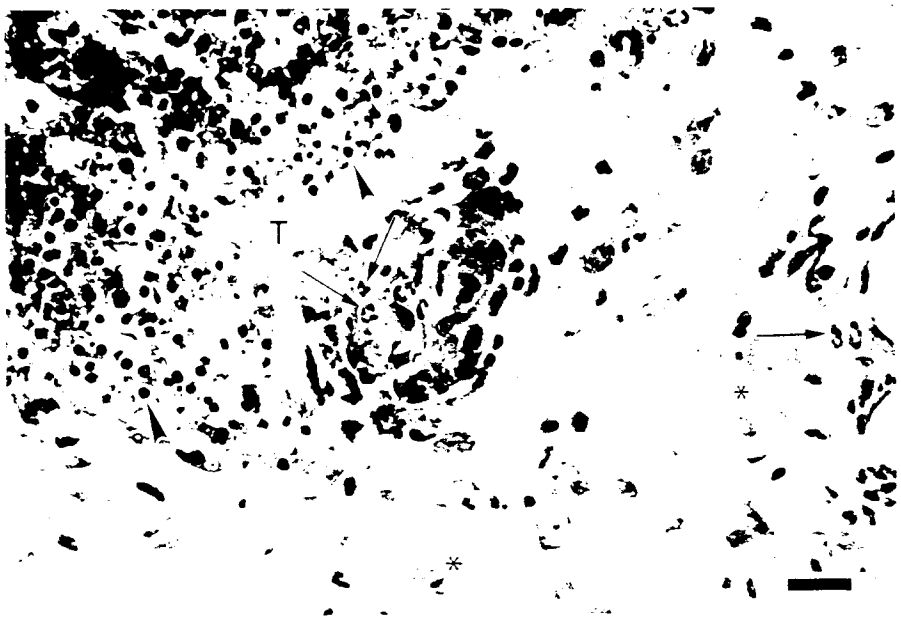

Fig 14. SP110. High magnification of the tip (T) of pulsed electrode # 2 shows numerous lymphocytes (arrowheads) and neutrophils within the infiltrate and also near post-capillary venules (arrows). Reactive astrocytes are also shown (*). Bar = 50 µm.

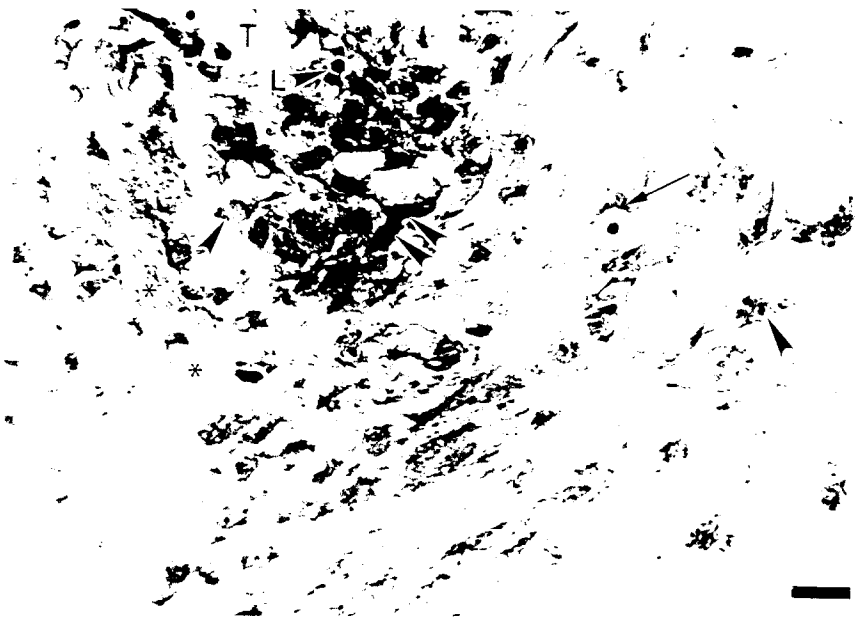

Figure 15. SP110. High magnification of the tip (T) of pulsed electrode #4. Note the spongy changes of the neuropil (*), reactive astrocytes (arrowheads), a vacuolated neuron (arrow), a shrunken neuron (double arrowheads) and a few lymphocytes near the tip (L + arrowhead). Stimulus parameters: 20 Hz, 100 µA, 400 µs/phase, 20% duty cycle. Bar = 50 µm.

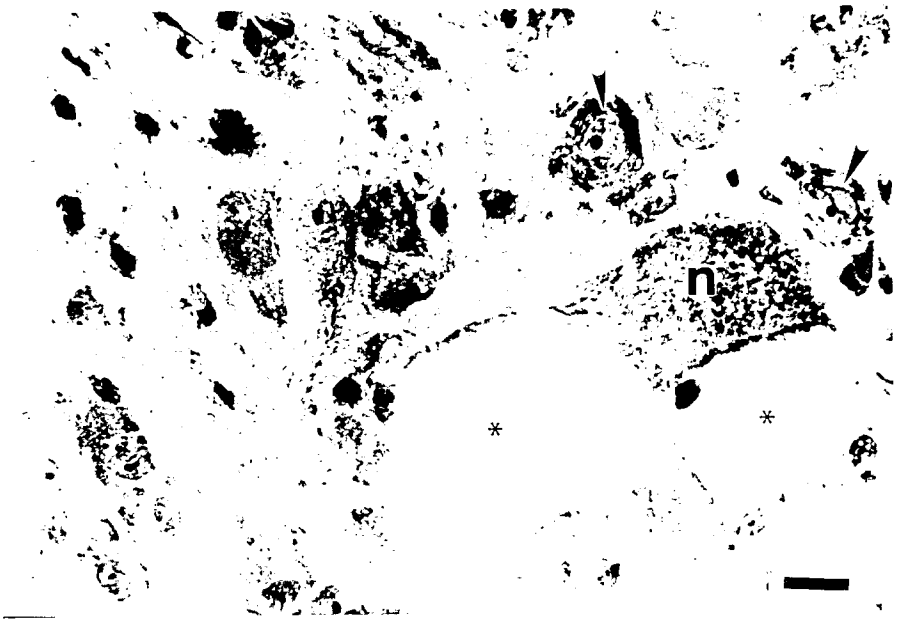

Figure 16. SP110. Approximately 500 µm distant to the tip of electrode #4, showing a portion of a large neuron (n) with perineuronal edema (*) adjacent to normal-appearing neurons (arrowheads). Bar = 50 µm.

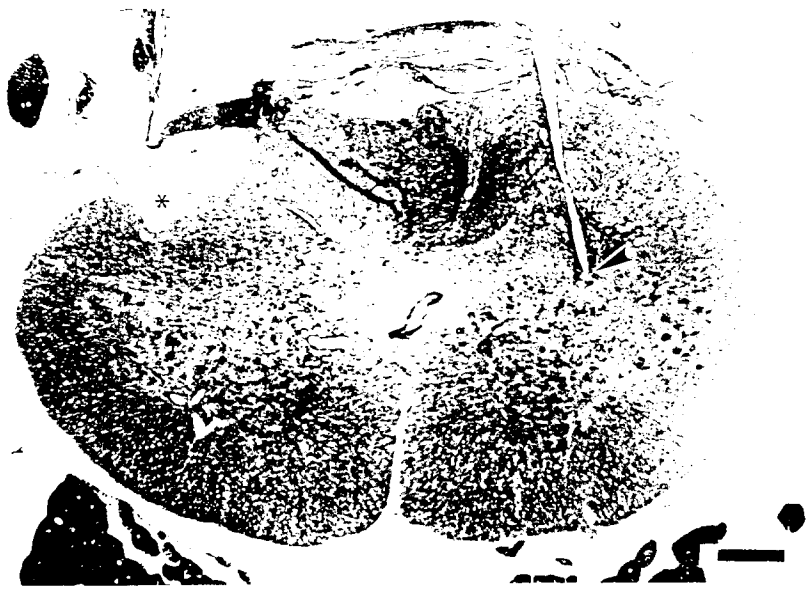

Figure 17. SP111. The track of unpulsed electrode #4 is shown (arrowhead). Note the compression of the dorsal surface of the opposite side of the cord (*). Bar = 500 µm.

Figure 18. SP111. The site of the tip (T) of unpulsed electrode #4, showing a normal-appearing neuron (n), gliosis (*) and a few leukocytes (arrowheads). Bar = 50 µm.

Figure 19. SP111. The track of pulsed electrode #5 (arrowhead). Note the compression of the dorsal surface of the cord (*). Stimulus parameters: 20 Hz, 100 µA, 400 µs/phase, 100% duty cycle, Bar = 500 µm.

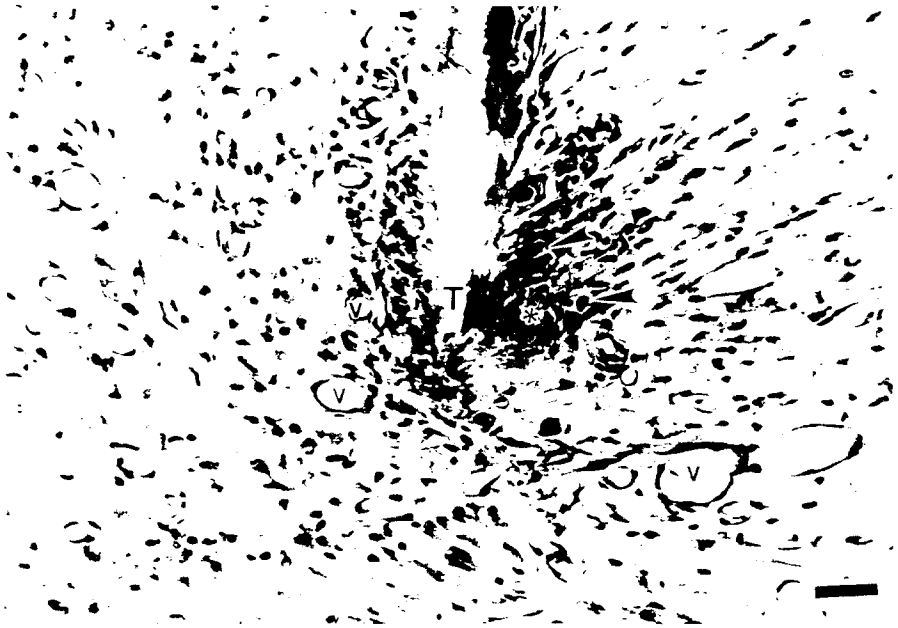

Figure 20. SP111. Higher magnification of the site of the tip (T) of pulsed electrode #5. Note the neovascularization (v), the accumulation of small lymphocytes (arrowheads) and a focus of reactive astrocytosis (*). Bar = 100 µm.

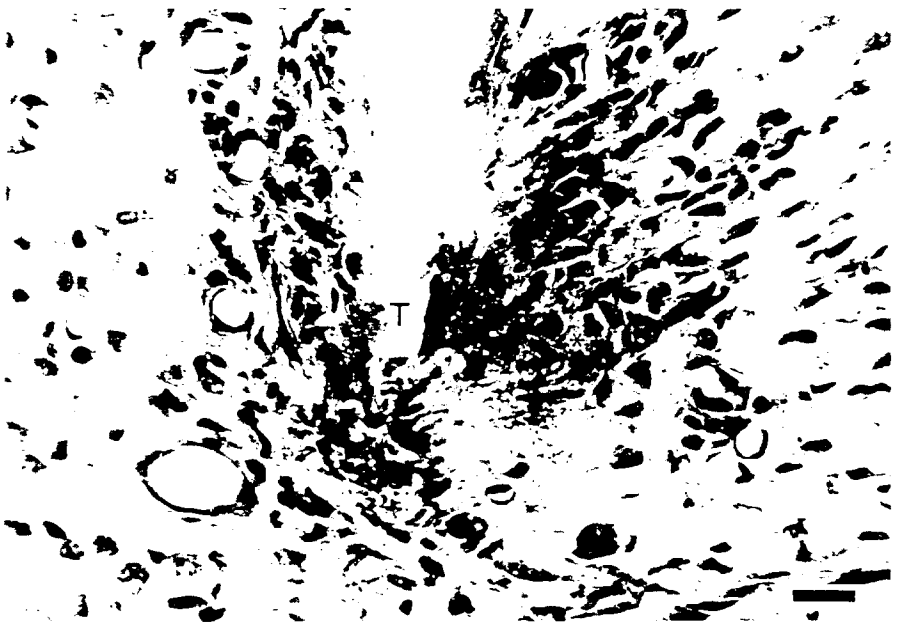

Figure 21. SP111. High magnification of the site of the electrode tip (T) shown in Figure 20. This figure shows the mixture of lymphocytes and astrocytes (*) adjacent to the tip. Identifiable neurons or their remnants are not present within the lesion. Bar = 50 µm.

Figure 22. SP111. The track and tip site of pulsed electrode # 3 (arrowhead). Note the accumulation of darkly-stained cells near the tip site. Stimulus parameters: 20 Hz, 100 µA, 400 µs/phase, 20% duty cycle. Bar = 500 µm.

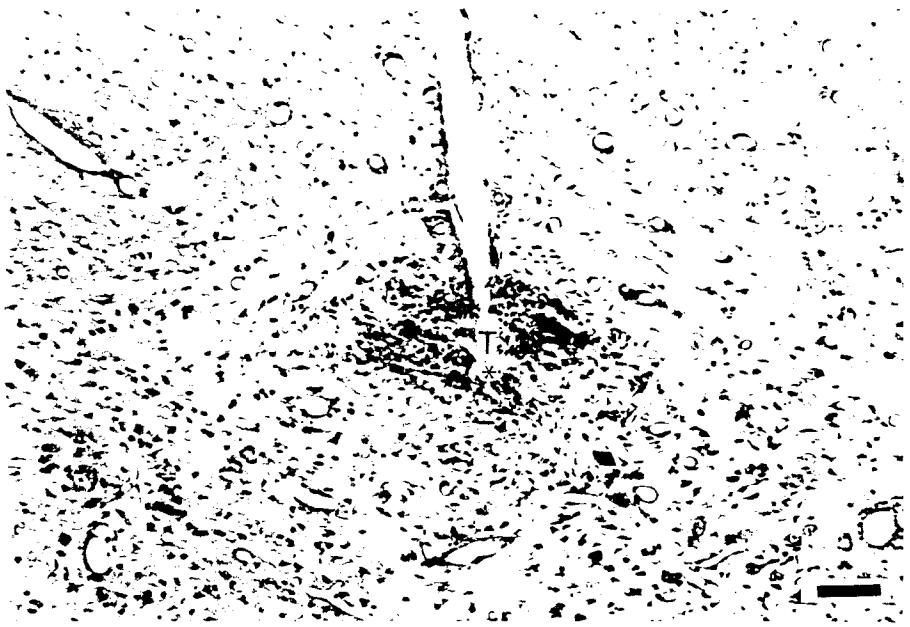

Figure 23. SP111. Higher magnification of the track (T) and site of the tip (*) of pulsed electrode #3. The electrode tip site is surrounded by reactive astrocytes and a few lymphocytes. Bar = 100 µm.

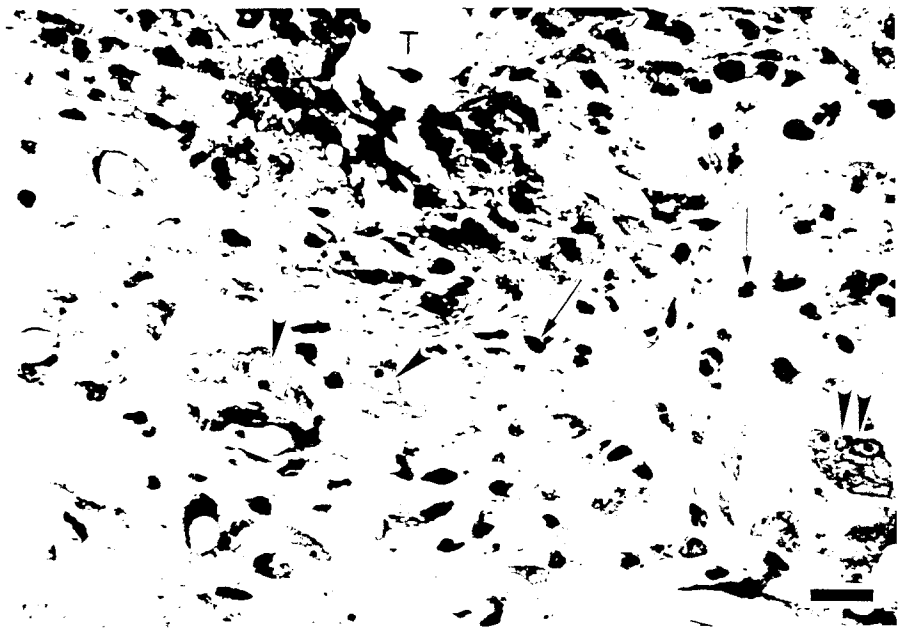

Figure 24. SP111. High magnification of the tip (T) of pulsed electrode #3, showing neurons (arrowheads), a few lymphocytes (arrows) and an apparent multinucleated giant cell (double arrowhead). Bar = 50 µm.

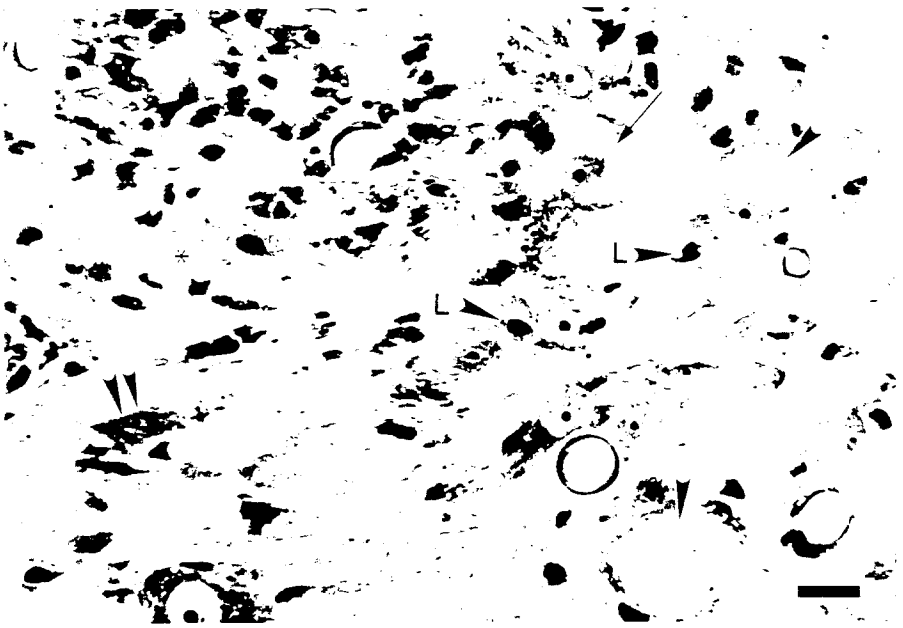

Figure 25. SP111. A section approximately 63 µm lateral to the actual tip of pulsed electrode # 3 and through the lesion surrounding the tip site (*). Some of the neurons show evidence of injury including two with chromatolytic changes (arrowheads), while others appear swollen (arrow) or darkened (double arrowheads). Some small lymphocytes are also shown (L + arrowheads). Bar = 50 µm.

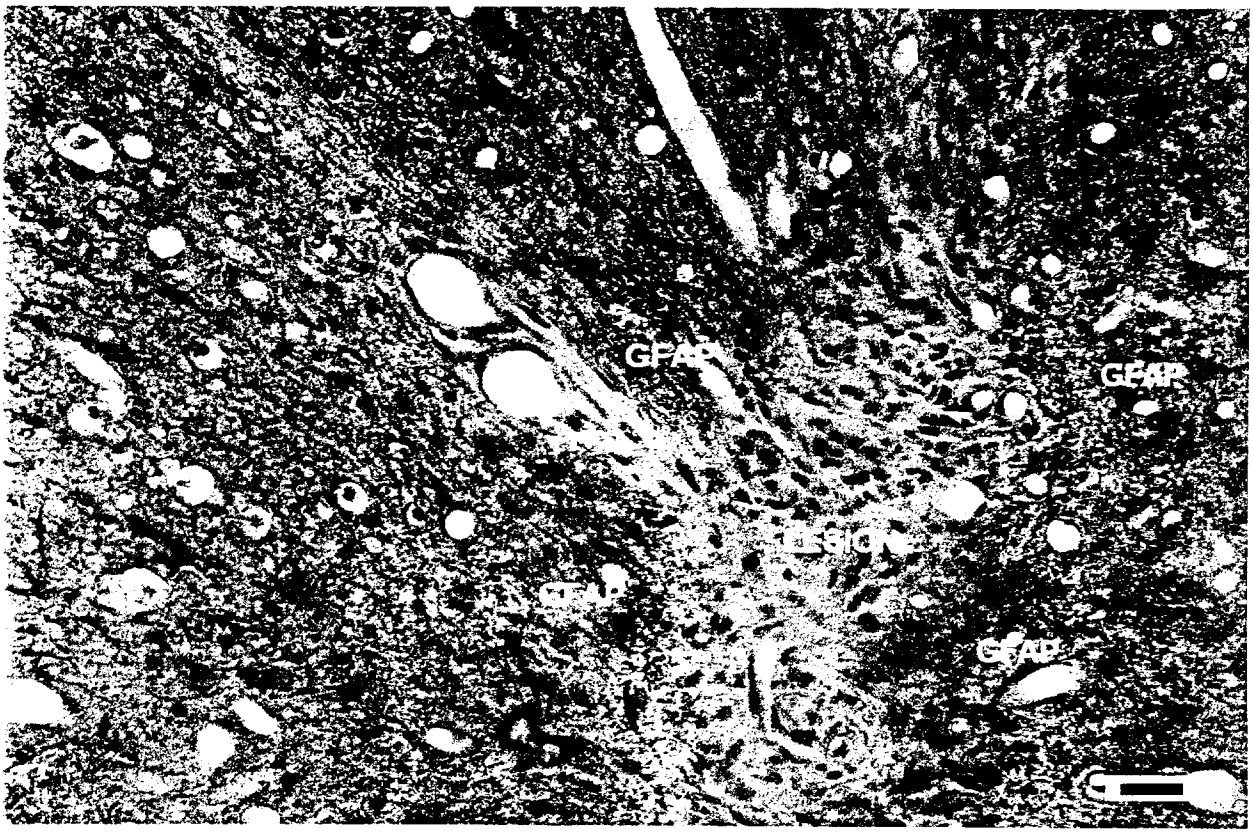

Figure 26. Animal SP111. A histologic section stained for the astrocyte marker GFAP. The section is through the lesion surrounding the tip of pulsed electrode #1, and is approximately 30 µm lateral to the electrode track and the actual tip site. The tissue immediately surrounding the lesion stains strongly for GFAP, but the protein is not detectable within the lesion. Bar = 100 µm.